http://dx.doi.org/10.5012/bkcs.2012.33.3.901

Effect of Pore Geometry on Gas Adsorption: Grand Canonical Monte Carlo Simulation Studies†

Eonji Lee, Rakwoo Chang,* Ji-Hyung Han,‡ and Taek Dong Chung‡

*Department of Chemistry, Kwangwoon University, Seoul 139-701, Korea. * E-mail: rchang@kw.ac.kr*
‡Department of Chemistry, Seoul National University, Seoul 151-747, Korea
Received November 30, 2011, Accepted January 5, 2012

In this study, we investigated the pure geometrical effect of porous materials in gas adsorption using the grand canonical Monte Carlo simulations of primitive gas-pore models with various pore geometries such as planar, cylindrical, and random pore geometries. Although the model does not possess atomistic level details of porous materials, our simulation results provided many insightful information in the effect of pore geometry on the adsorption behavior of gas molecules. First, the surface curvature of porous materials plays a significant role in the amount of adsorbed gas molecules: the concave surface such as in cylindrical pores induces more attraction between gas molecules and pore, which results in the enhanced gas adsorption. On the contrary, the convex surface of random pores gives the opposite effect. Second, this geometrical effect shows a nonmonotonic dependence on the gas-pore interaction strength and length. Third, as the external gas pressure is increased, the change in the gas adsorption due to pore geometry is reduced. Finally, the pore geometry also affects the collision dynamics of gas molecules. Since our model is based on primitive description of fluid molecules, our conclusion can be applied to any fluidic systems including reactant-electrode systems.

Key Words : Pore geometry, Gas adsorption, Grand canonical Monte Carlo simulation

Introduction

Gas adsorption in porous materials has recently attracted much interest in both industry and academia because of its various applications to the separation, sequestration, and storage of gases such as H_2, CH_4, and CO_2.[1-7] For example, the development of efficient CO_2 capture and sequestration (CCS) techniques using porous materials is actively in progress because of worldwide concerns over global warming by greenhouse gas emission.[8,9] In addition, safe and pollution-free vehicles using H_2 fuels require effective H_2 storage devices.[10] Hence, researchers have made immense efforts to find new gas adsorption materials for these purposes.[11-13] Especially, the microporous materials such as metal-organic frameworks (MOFs), carbon nanotubes (CNTs), zeolites, and graphenes have been intensively investigated as the potential candidate because of their high gas selectivity, high surface area, and high thermal stability.[14-16]

However, there still remain many challenging issues to overcome in developing efficient gas adsorption materials. One issue is that the differences in physical properties of gases that should be separated (CO_2, H_2, N_2, and CH_4) are relatively small as can be expected in their kinetic diameters.[17,18] Another issue to overcome is that the selectivity of the gas adsorption process is controlled by both solubility (or absorption) and diffusivity, which are inversely correlated.[19] Other issues include reversible adsorption and desorption control, thermal and high pressure stabilities, and so on. These challenging issues require the molecule-level control of gas adsorption materials that can make full use of slight differences in physical and chemical properties and independently tune solubility and diffusivity of gas molecules.

The gas adsorption in porous materials is usually affected by many factors such as gas-pore interaction, pore size, pore morphology, and surface roughness.[20,21] Among those, the effect of pore morphology on gas adsorption has been studied extensively using grand canonical Monte Carlo (GCMC) simulations.[22-25] Bohlena *et al*. investigated the impact of surface curvature of substrate on the phase behavior of an adsorbing fluid.[22] Puibasset *et al*. also studied adsorption and desorption behavior of a Lennard-Jones fluid in cylindrical pores with various chemical heterogeneities.[23]

However, the direct comparison of gas adsorption in various pore shapes such as flat, cylindrical, and random pores to investigate the effect of pure pore geometry on the gas adsorption has been rare. Hence, in this study, we performed the grand canonical Monte Carlo simulations of primitive gas-pore models with various pore geometries.

This paper is organized as follows. In the methods section, the molecular model and computer simulation methods used in this study are described in detail. The structural, dynamical, and thermodynamic analyses are then presented in the results and discussion section, while a summary and conclusions are given in the conclusion section.

Methods

We employed Grand Canonical Monte Carlo Simulations

†This paper is to commemorate Professor Kook Joe Shin's honourable retirement.

(GCMC) to study the effect of pore geometry on the adsorption of fluid gas molecules on the surface of porous materials. The gas molecules are modeled as Ar molecules of spherical shape and the pore materials as a solid structure. Three different surface geometries were investigated in this study: planar, cylindrical, and random pores. The planar pore geometry is modeled as a slit, the width of which is set to L = 4 nm, and the cylindrical pore geometry as a cylindrical pipe with radius of R = 2 nm or 4 nm. For random pore geometries,[26] hard spheres with the diameter of $\sigma = 3$ nm are equilibrated in a given volume fraction ϕ ($\equiv \pi/6\rho_{pore}\sigma^3$) and then immobilized in the space.

Periodic boundary condition in the directions without a wall is applied to each system to minimize the finite-size effect. For example, the cylindrical pore is infinitely long in the z direction and the planar pore is infinite in both x and y directions. On the other hand, the random pore is infinite in all directions. Figure 1 shows the three porous geometries along with fluid gas molecules.

The interaction between Ar molecules is represented by the Lennard-Jones potential with parameters $\varepsilon_{LJ} = 0.2465$ kcal/mol and $\sigma_{LJ} = 0.342$ nm.

The interaction between gas molecules and porous materials (substrate) is described as the sum of the Lennard-Jones interactions between them:

$$U(\vec{r}) = 4\varepsilon_s\rho_s \int_{\vec{s}\in substrate} d\vec{s}\left[\left(\frac{\sigma_s}{|\vec{r}-\vec{s}|}\right)^{12} - \left(\frac{\sigma_s}{|\vec{r}-\vec{s}|}\right)^{6}\right],$$

where ε_s and σ_s are the Lennard-Jones parameters between a gas molecule and an atom consisting of the porous material, and ρ_s is the number density of atoms in the porous material.

For simple surface geometries, $U(\vec{r})$ can be obtained in an analytical form.[27] For example, for planar geometry,

$$U_{plane}(r) = 4\varepsilon_s\rho_s \int_0^{2\pi} d\phi \int_0^{\infty} ds \int_0^{\infty}\left[\left(\frac{\sigma_s}{\sqrt{r^2+s^2}}\right)^{12} - \left(\frac{\sigma_s}{\sqrt{r^2+s^2}}\right)^{6}\right]$$

$$= D\left[\frac{4}{27}\left(\frac{d}{r}\right)^9 - \left(\frac{d}{r}\right)^3\right],$$

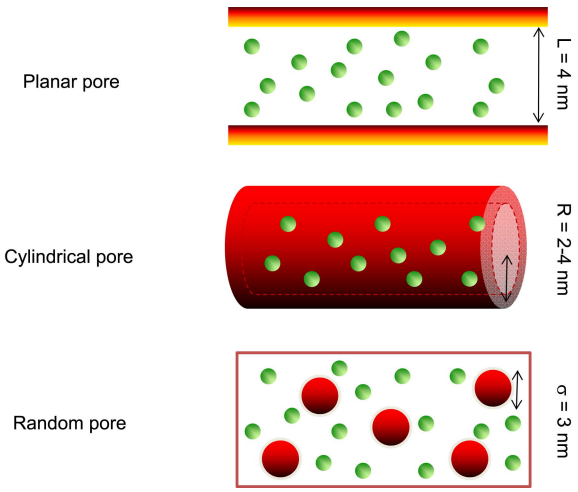

Figure 1. Three different pore geometries. Green spheres represent gas molecules.

where r is the shortest distance between the gas molecule and the porous surface, and both the interaction energy D ($\equiv\sqrt{40}\pi/9\ \rho_s\varepsilon_s\sigma_s^3$) and the interaction length d ($\equiv(C/D)^{1/3}$) depend on the porous materials. The parameter C in the above expression is defined as $(2\pi/3)\rho_s\varepsilon_s\sigma_s^6$ and corresponds to the asymptotic van der Waals interaction coefficient: i.e., $U_{plane}(r) \approx -C/r^3$ at large r. It is noted that the potential has a minimum energy of $-D$ at $r_{min} = (2/3)^{1/3}d$ and zero at $r_0 = (4/27)^{1/6}d$.

For Ar molecules, the parameter C ranges from 0.014 (kcal/mol)·nm^3 (alkali metal and insulators) to 0.040 (kcal/mol)·nm^3 (transition metals).[28] In this study, d is set to 0.23 nm and D varies from 0.1 to 10 kcal/mol, spanning the broad interaction range. On the other hand, the system temperature is set to 298 K.

Similarly, for cylindrical and random porous geometries, the attractive part of the gas-pore interaction is respectively given by

$$U^{att}_{cylinder}(r) = -\frac{3\pi}{2}\frac{C}{R^3}F\left(\frac{3}{2}, \frac{5}{2}; 1; y^2\right)$$

and

$$U^{att}_{cylinder}(r) = -\frac{C}{(1+r/2R)^3 r^3},$$

where F is a hypergeometric function, R is the radius of a cylindrical pore or random spheres, and y ($\equiv -r/R$) is the reduced distance of the gas molecule from the axis of the cylindrical pore.

On the other hand, for the short-ranged repulsive part of the interactions we have adopted that of the planar surface geometry:

$$U^{rep}_{plane}(r) = U^{rep}_{cylinder}(r) = U^{rep}_{random}(r) = \frac{4D}{27}\left(\frac{d}{r}\right)^9$$

We do not expect this approximation to affect our results significantly.

Using this primitive model, we performed GCMC simulations to sample equilibrium configurations of fluid molecules in pore geometries. Typical trial moves such as translation, molecule creation, and molecule deletion moves were employed and accepted according to Metropolis' algorithm.[29] Each system was equilibrated until both the system potential energy and the density of gas molecules in the system did not drift any more.

Once the system was equilibrated, at least 3000 snapshots of equilibrated system configurations were sampled depending on the interaction strength and used for the structural analysis. The results given in this study are the averages of these configurations and the error bar, obtained from block averaging, corresponds to one standard deviation from the average.

Results and Discussion

Figure 2 shows the concentration profiles of Lennard-Jones gas molecules near the surface of various pore geo-

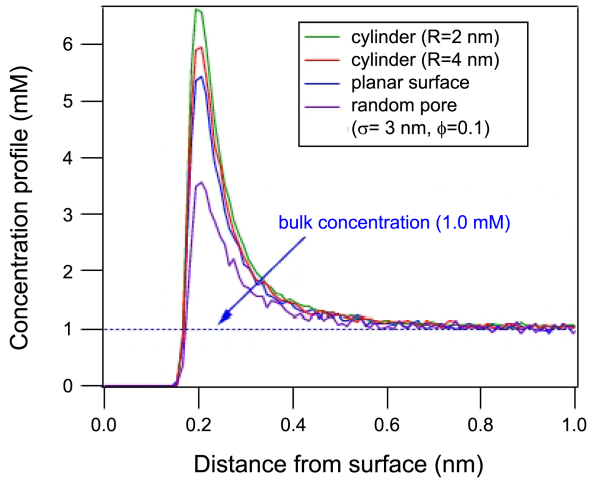

Figure 2. Concentration profile near the surface for various pore geometries at the bulk gas concentration of 1.0 mM, which corresponds to the gas pressure of 0.024 atm. Gas-pore interaction parameters d and D are set to 0.23 nm and 1.0 kcal/mol, respectively.

metries for bulk gas concentration of 1.0 mM, which corresponds to the gas pressure of 0.024 atm, and the interaction parameter $D = 1.0$ kcal/mol. For all pore geometries, a strong peak appears around 0.2 nm from the pore surface, which is the signature of the van der Waals attraction between the gas molecules and porous materials, and the peak is followed by a slow decay to the bulk concentration around 0.6 nm. The peak height is directly related to the surface curvature around the reactants: As the surface gets more concave inwards, the peak gets stronger. It is expected because gas molecules feel stronger van der Waals attraction from the porous material as they are more closely surrounded by its surface.

From the concentration profile we can calculate the adsorption excess per unit area, Γ_{ex}, defined as

$$\Gamma_{ex} \equiv \frac{1}{A_{surface}} \int [c(\vec{r}) - c_{bulk}] d\vec{r},$$

where $A_{surface}$ is the accessible pore surface area, $c(\vec{r})$ the gas concentration, and c_{bulk} the bulk gas concentration. Both the accessible surface area and the accessible volume were measured using the minimum distance r_0 ($\equiv (4/27)^{1/6} d$ = 0.167 nm) of the gas-pore interaction. Γ_{ex} is a measure of the excess amount of the gas concentration in the presence of the porous material relative to the system without porous materials.

Figure 3(a) shows Γ_{ex} as a function of the van der Waals interaction parameter D for various pore geometries. It is noted that the plot is drawn on a log-log scale. It is clear that as the van der Waals interaction D is increased, the excess adsorption becomes stronger. At low D (i.e. when the gas-pore interaction is small), Γ_{ex} increases weakly with increasing D but it starts rising steeply from $D > 1$ kcal/mol. This behavior is well known as the wetting transition or capillary condensation.[26]

On the other hand, as discussed in the previous section, the pore surface curvature plays a significant role in the fluid gas

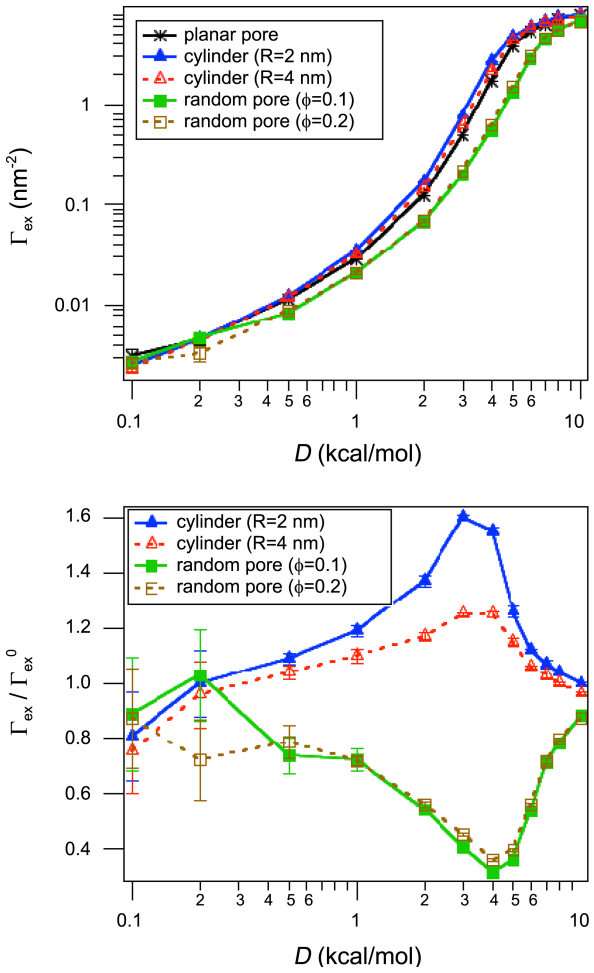

Figure 3. (a) Adsorption excess per unit area Γ_{ex} as a function of gas-pore interaction strength D for various pore geometries. The bulk fluid gas concentration is 1 mM and the gas-pore interaction length d is set to 0.23 nm. (b) $\Gamma_{ex}/\Gamma^0_{ex}$ as a function of gas-pore interaction strength D for various pore geometries. Γ^0_{ex} is the adsorption excess per unit area for planar pore geometry.

adsorption on its surface: The more concave is the pore surface, the stronger gas adsorption occurs on the surface. It should be emphasized that the difference in the adsorption for a given D is entirely due to the pore surface geometry. This is clearly seen in Figure 3(b), where we plot the excess adsorption isotherm (Γ_{ex}) for various pore geometries relative to that of planar pore geometry (Γ^0_{ex}). For cylindrical pore geometries (concave inwards in the middle), Γ_{ex} is larger than Γ^0_{ex} in most cases except when D is very small, but the trend is reversed for random pore geometries, which have convex surface. This geometrical effect on the adsorption is augmented up to $D \sim 4$ kcal/mol and then diminishes at higher D. The decrease at high D is due to the fact that the excluded volume repulsion among crowded gas molecules adsorbed on the pore surface starts playing a role in the adsorption process in addition to the van der Waals attraction between the gas molecule and the porous material.

The gas-pore interaction length d also has a significant effect on the adsorption behavior of gas molecules. Figure 4(a) and (b) show both absolute (Γ_{ex}) and relative ($\Gamma_{ex}/\Gamma^0_{ex}$)

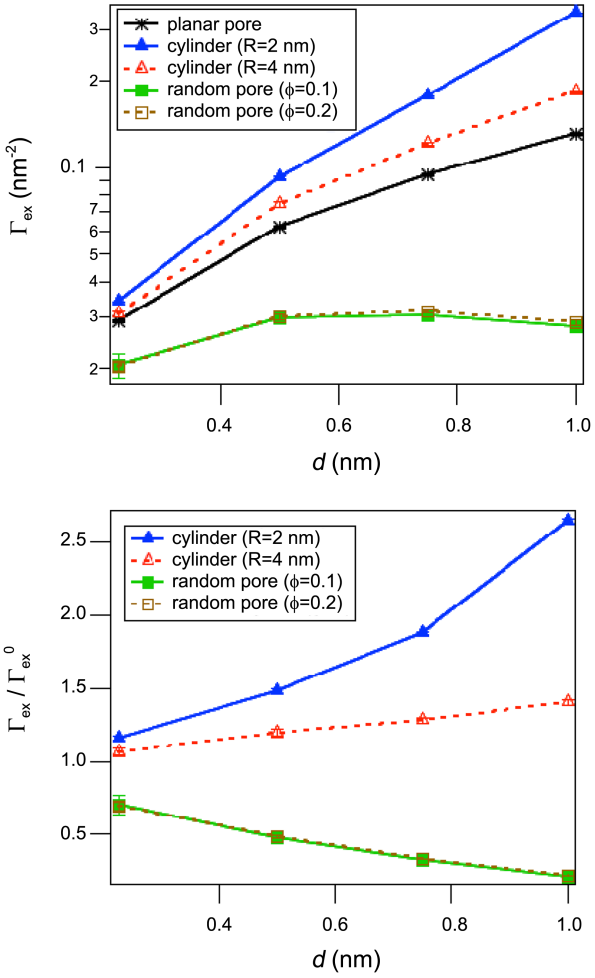

Figure 4. (a) Adsorption excess per unit area Γ_{ex} as a function of gas-pore interaction length d for various pore geometries. The bulk fluid gas concentration is 1 mM and the gas-pore interaction strength D is set to 1.0 kcal/mol. (b) $\Gamma_{ex}/\Gamma^0_{ex}$ as a function of gas-pore interaction length d for various pore geometries. Γ^0_{ex} is the adsorption excess per unit area for planar pore geometry.

adsorption excesses as a function of d. In both planar and cylindrical pore geometries, Γ_{ex} increases monotonically from d = 0.23 nm to d = 1 nm. It implies that the van der Waals attraction from neighboring surface atoms get stronger with increasing the interaction length. It is noted that the interaction range, which can be estimated in the density profiles near the surface (data not shown), increases from 0.6 nm (d = 0.23 nm) to 1.5 nm (d = 0.5 nm) over 2.0 nm (d > 0.75 nm).

On the other hand, Γ_{ex} initially increases but starts decreasing with larger d values, where additional factor plays a negative effect on the gas adsorption: With increasing d, the available space for gas molecules becomes smaller. For example, the plateau gas concentration in the density profile at the random pore geometry with $\phi = 0.2$ is around 100 times lower than the corresponding bulk concentration.

As a result, the effect of pore geometry on the gas adsorption becomes stronger with longer gas-pore interaction length, which is clearly seen in Figure 4(b). The relative gas adsorption in cylindrical pores is more pronounced with

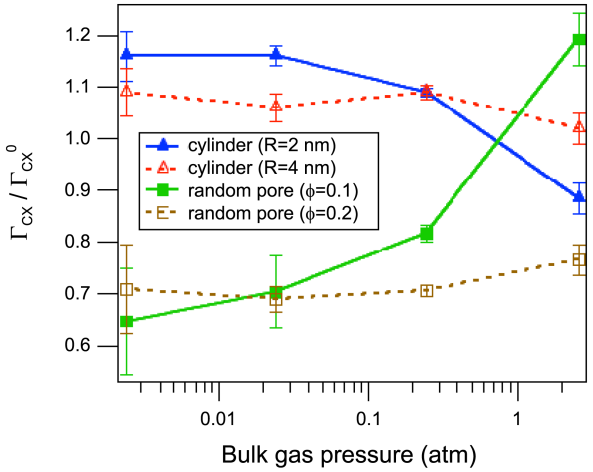

Figure 5. $\Gamma_{ex}/\Gamma^0_{ex}$ as a function of gas pressure for various pore geometries. Γ^0_{ex} is the adsorption excess per unit area for planar pore geometry. The gas-pore interaction parameters d and D are set to 0.23 nm and 1.0 kcal/mol, respectively.

increasing d but random pores show the opposite trend.

Another factor affecting the gas adsorption in porous materials is the crowding effect. With increasing the gas pressure (or bulk concentration), the interaction between the gas molecules starts competing with the interaction between the gas molecule and pore. This competition is expected to diminish the pure geometrical effect of the gas adsorption. Figure 5 displays the relative adsorption excess as a function of the gas pressure for various pore geometries. As expected, the relative adsorption excess of cylindrical pores decreases with increasing gas pressure. Since the inter-molecular interaction becomes dominant over the gas-pore interaction at high pressure (or concentration), the surface curvature of the pore geometry now plays an opposite role: the concave (convex) surface drives gas molecules closer (farther apart) than the corresponding planar surface, which results in the decrease (increase) in the relative adsorption excess.

Finally, to study the effect of pore geometry on the reactivity of the porous materials, we have also calculated the collision rate v_{coll} of a single molecule for various pore geometries using conventional Monte Carlo simulations with only translational move. In the simulation, the single molecule moves by random walk with the step size of 0.15, the time step of 0.0375 ps, and the diffusion coefficient of 0.1 cm^2/s. Each trial move is accepted or rejected based on the Metropolis algorithm.[29] At each step we check whether the molecule collides with the pore surface. We assume that the collision occurs when the shortest distance between the molecule and the surface is less than $(C/k_BT)^{1/3}$, where k_B is the Boltzmann constant and T = 298 K.

The results are given in Figure 6 as a function of the interaction parameter D. The collision rate v_{coll} increases steeply in the range of D = 1-3 kcal/mol and reaches a plateau (33 ps^{-1}). The reason why v_{coll} has a plateau at high D is because the molecule is trapped near the surface most of the time during the whole simulation at this high D. Therefore, the maximum of v_{coll} is limited by the sampling

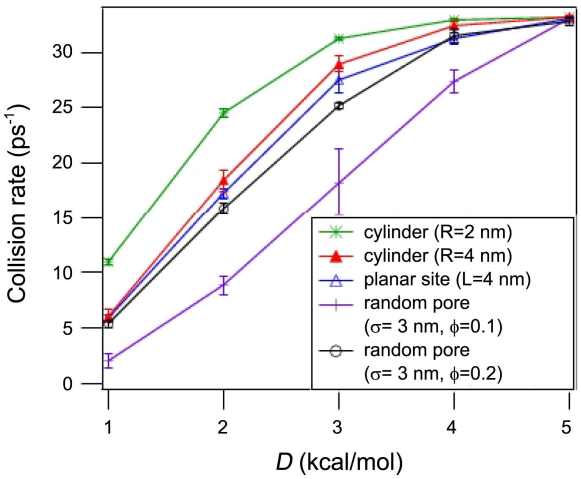

Figure 6. Collision rate v_{coll} for various pore geometries.

frequency of the simulation. On the other hand, unlike Γ_{ex}, v_{coll} is strongly dependent on the volume fraction $\phi^{1/3}$ of the random porous geometry. This is because the average distance between random spheres is inversely proportional to $\phi^{1/3}$ and the gas molecule encounters the random spheres more frequently at high ϕ.

Conclusion

In this study, we investigated the pure geometrical effect of porous materials in gas adsorption using the grand canonical Monte Carlo simulations of primitive gas-pore models with various pore geometries such as slitlike, cylindrical, and random pore geometries.

Although the model does not possess atomistic level details of porous materials, our simulation results provided many insightful information in the effect of pore geometry on the adsorption behavior of gas molecules.

First, the surface curvature of porous materials plays a significant role in the amount of adsorbed gas molecules: the concave surface such as in cylindrical pores induces more attraction between gas molecules and pore, which results in the enhanced gas adsorption, compared to planar pores. On the other hand, the convex surface of random pores, which are observed in experiments such as electro-deposited Pt microelectrodes,[30] gives the opposite effect.

Second, this geometrical effect shows a nonmonotonic dependence on the gas-pore interaction strength D. For example, the concave pore surface such as in cylindrical pores enhances the relative gas adsorption up to D = 3-4 kcal/mol, but starts diminishing with higher interaction strength, where the crowding effect of gas molecules near the surface plays a dominant role. In addition, the gas-pore interaction length d also has a significant effect on the adsorption behavior gas molecules by controlling the range of van der Waals attraction between gas molecules and pore materials.

Third, the crowding effect of gas molecules competes with the gas-pore interaction. So, as the external gas pressure (or concentration) is increased, the enhancement (or decrease) in the gas adsorption due to pore geometry is reduced.

Finally, the pore geometry also affects the collision dynamics of gas molecules, which can lead to the change in the reactivity of the molecules on the surface in reactive systems.

As a final note, it should be emphasized that our conclusion can be applied to any fluidic systems such as reactant-electrode systems in solution because our model does not assume gas-specific conditions.

Acknowledgments. We would like to thank Professor Kook Joe Shin of Seoul National University for his endless passion and numerous contributions to statistical thermodynamics. This work was supported by the Korea Research Foundation grant funded by the Korean Government (MEST) (No. 2010-0003087).

References

1. Li, W.; Hoa, N. D.; Kim, D. *Sensors and Actuators B: Chemical* **2010**, *149*, 184.
2. Li, C.; Su, Y.; Lv, X.; Xia, H.; Wang, Y. Sensors *and Actuators B: Chemical* **2010**, *149*, 427.
3. Lee, J. Y.; Olson, D. H.; Pan, L.; Emge, T. J.; Li, J. *Adv. Funct. Mater.* **2007**, *17*, 1255.
4. Belmabkhout, Y.; Serna-Guerrero, R.; Sayari, A. *Ind. Eng. Chem. Res.* **2010**, *49*, 359.
5. Liu, Y.; Liu, H.; Hu, Y.; Jiang, J. *J. Phys. Chem. B* **2009**, *113*, 12326.
6. Gallo, M.; Glossman-Mitnik, D. *J. Phys. Chem. C* **2009**, *113*, 6634
7. Caskey, S. R.; Wong-Foy, A. G.; Matzger A. J. *J. Am. Chem. Soc.* **2008**, *130*, 10870.
8. Xu, X.; Xiao, Y.; Qiao, C. *Energy & Fuels* **2007**, *21*, 1688.
9. Reddy, M. K. R.; Xu, Z. P.; Lu, G. Q.; Da Costa, J. C. D. *Ind. Eng. Chem. Res.* **2006**, *45*, 7504.
10. Babarao, R.; Eddaoudi, M.; Jiang, J. W. *Langmuir* **2010**, *26*, 11196.
11. Düren, T.; Sarkisov, L.; Yaghi, O. M.; Snurr, R. Q. *Langmuir* **2004**, *20*, 2683.
12. McKinlay, A. C.; Xiao, B.; Wragg, D. S.; Wheatley, P. S.; Megson, I. L.; Morris, R. E. *J. Am. Chem. Soc.* **2008**, *130*, 10440.
13. Meng, S.; Kaxiras, E.; Zhang, Z. *Nano. Lett.* **2007**, *7*, 663.
14. Krishna, R. *J. Phys. Chem. C* **2009**, *113*, 19756.
15. Xiang, Z.; Lan, J.; Cao, D.; Shao, X.; Wang, W.; Broom, D. P. *J. Phys. Chem. C* **2009**, *113*, 15106.
16. Roussel, T.; Didion, A.; Pellenq, R. J.-M.; Gadiou, R.; Bichara, C.; Vix-Guterl, C. *J. Phys. Chem. C* **2007**, *111*, 15863.
17. Roman-Perez, G.; Moaied, M.; Soler, J. M.; Yndurain, F. *Phys. Rev. Lett.* **2010**, *105*, 145901.
18. Park, H. J.; Suh, M. P. *Chem. Commun.* **2010**, *46*, 610.
19. Arora, G.; Wagner, N. J.; Sandler, S. I. *Langmuir* **2004**, *20*, 6268.
20. Porcheron, F.; Schoen, M.; Fuchs, A. H. *J. Chem. Phys.* **2002**, *116*, 5816.
21. Coasne, B.; Pellenq, R. J.-M. *J. Chem. Phys.* **2004**, *120*, 2913.
22. Bohlena, H.; Schoen, M. *J. Chem. Phys.* **2005**, *123*, 124714.
23. Puibasset, J. *J. Chem. Phys.* **2006**, *125*, 074707.
24. Coasne, B.; Galarneau, A.; Renzo, F. D.; Pellenq, R. J. M. *Langmuir* **2010**, *26*, 10872.
25. Ma, Q.; Yang, Q.; Zhong, C.; Mi, J.; Liu, D. *Langmuir* **2010**, *26*, 5160.
26. Chang, R.; Jagannathan, K.; Yethiraj, A. *Phys. Rev. E* **2004**, *69*, 051101.
27. Gatica, S. M.; Cole, M. W. *Phys. Rev. E* **2005**, *72*, 041602.
28. Vidali, G.; Ihm, G.; Kim, H. Y.; Cole, M. W. *Surf. Sci. Rep.* **1991**, *12*, 133.
29. Allen, M. P.; Tildesley, D. J. *Computer Simulation of Liquids*; New York, 1987.
30. Han, J.-H.; Lee, E.; Park, S.; Chang, R.; Chung, T. D. *J. Phys. Chem. C* **2010**, *114*, 9546.